Si stable isotope fractionation during adsorption and the competition between kinetic and equilibrium isotope fractionation: implications for weathering systems

Marcus Oelze, Friedhelm von Blanckenburg, Daniel Höllen, Martin Dietzel, Julien Bouchez

Si stable isotope fractionation during adsorption and the competition between kinetic and equilibrium isotope fractionation: Implications for weathering systems

Marcus Oelze [a,*], Friedhelm von Blanckenburg [a,c], Daniel Hoellen [b], Martin Dietzel [b], Julien Bouchez [a]

[a] *Helmholtz Centre Potsdam, GFZ German Research Centre for Geosciences, Germany*
[b] *Institute of Applied Geosciences, Graz University of Technology, Austria*
[c] *Department of Geoscience, Freie Universität Berlin, Germany*

1. Introduction

Weathering of minerals and rocks releases elements into the ambient solution. Si and Al being the second and third most abundant elements in the Earth's crust, respectively, are both key players during weathering of silicates. While Al is almost insoluble under near neutral pH conditions and low dissolved organic carbon contents (Sposito, 1996), Si is partitioned in roughly equal proportions between the dissolved phase and into a solid secondary mineral phase during the dissolution of primary silicate minerals. In the last decade Si stable isotopes have been increasingly used to trace weathering processes.

One major finding of these Si isotope studies is the relative enrichment of heavy Si isotopes in the ambient soil solution. The isotopically lighter counterpart is found in secondary siliceous solid phases (Ziegler et al., 2005a,b; Georg et al., 2006a, 2007; Opfergelt et al., 2009; Bern et al., 2010; Opfergelt et al., 2011). Despite this consistent picture, the partitioning of Si isotopes in the presence of Al has not been explored in detail under controlled laboratory conditions. Determining the related isotope fractionation factors is critical as the reaction of Si and Al is likely to be the first crucial reaction occurring in weathering environments after releasing Al and Si from primary silicates.

In the present study, we explore Si isotope fractionation during adsorption of Si onto gibbsite at three different initial Si concentrations. We explain the resulting dependence of the Si isotope fractionation factor on adsorption rate within the conceptual mass balance framework of DePaolo (2011).

* Corresponding author.
 E-mail address: oelze@gfz-potsdam.de (M. Oelze).

2. Materials and methods

2.1. Si source for adsorption experiments

Dietzel (1993, 2002) showed that only monomeric silicic acid (H_4SiO_4) is formed when tetraethylorthosilicate (TEOS; ($C_2H_5O)_4Si$) is used as Si source and that its behavior in adsorption experiments is identical to that found in monomeric silicic acid solutions prepared by alternative means. The advantage of using TEOS as Si source is that neither associated cations nor minor elemental amounts (released during the dissolution of silicates (e.g. Na_2SiO_3) or from alkaline standard solutions (SiO_2 in 2% NaOH)) are present in the solution, which then have to be removed to obtain pure silicic acid for experiments. Further monomeric silicic acid can be produced easily by a simple addition of small volumes of TEOS to aqueous solutions where TEOS converts to silicic acid via a hydrolysis reaction. The side product of TEOS hydrolysis is ethanol (a concentration of 261 ppm is calculated). The Si stock solution was prepared by adding 5.9 g (6 ml) TEOS (Merck®) to 20 l Milli-Q water (1.42 mmol/l Si).

To avoid formation of polysilicic acid the prepared starting solution was held below the solubility of amorphous silica. In addition, before using the starting solution we first analyzed the solution for the degree of polymerization of dissolved silicic acid and the presence of colloidal silica using the β-silicomolybdate method (for details see Online Supplement B and Iler (1979) and Dietzel (2000)). The amount of colloidal silica is determined by measuring the total Si concentration using ICP-OES minus the concentration of monosilicic acid determined by the β-silicomolybdate method. For all experiments both Si concentrations show that within the analytical precision of 5% no colloidal Si was present in the experiments. Furthermore, the reaction rate constant for the formation of the β-silicomolybdate complex can be used to evaluate the average polymerization degree of dissolved silicic acid. For the present stock solution a value of 2 min^{-1} was calculated, which clearly indicates the sole presence of monomeric silicic acid.

2.2. Adsorption experiments

Adsorption experiments were carried out following a method adapted from Dietzel and Böhme (1997). The experimental solutions were prepared from a TEOS stock solution. Three distinct adsorption experiments were performed with initial Si concentrations of 0.36, 0.71 and 1.42 mmol/l Si corresponding to concentrations of 10, 20 and 40 ppm, respectively. All experimental solutions were adjusted to 0.1 M NaCl by addition of NaCl (p.a. grade Merck®). Si concentrations were below the solubility limit of amorphous silica which is 1.93 mmol/l Si at 25 °C and pH < 8 (Gunnarsson and Arnorsson, 2000), to prevent polymerization and precipitation of amorphous silica.

In each experimental run 30 g of gibbsite (γ-Al(OH)$_3$; p.a. grade Merck®) with a given specific surface area of 1.18 m^2/g (BET, N$_2$-adsorption) was suspended in 1 l of the experimental solution containing Si in PE bottles. The pH of 7.0 was adjusted and kept constant during the experiment by the addition of diluted HCl or NaOH solution (pH were measured with pH meter WTW 330 and pH electrode WTW SenTix 41, calibrated using pH 4.0 and 7.0 WTW standard buffer solutions). The variability of the pH values throughout the whole experimental runtime was ± 0.1 pH units. During the first 6 h of the experiment, the gibbsite suspension was heavily agitated using a IKA RW 20 DZM stirrer at 500 rpm with a Teflon stirring staff. A parafilm cover prevented evaporation of the solution. Subsequently the closed PE bottles were placed in an overhead shaker. Experimental suspensions (15 ml) were sampled with a syringe and filtered (0.45 μm porosity, cellulose acetate) at several intervals; total maximum experimental run time was 1536 h (64 days). The sampled solutions were split: 10 ml were used for ICP-OES analyses (Varian 720-ES) and Si isotope measurements (Thermo Scientific NEPTUNE). The remaining solutions of 5 ml were immediately analyzed by UV–Vis (UV–VIS 641 Cary 100, Varian).

2.3. Chemical separation and purification

Chemical separation of Si was done following the method from Georg et al. (2006b). The filtered solutions were loaded onto pre-cleaned columns (1.5 ml of BioRad DOWEX 50 W-X8; 200–400 mesh) and Si was eluted with 5 ml Milli-Q water and stored in pre-cleaned centrifuge tubes. It was assured for all samples that the Si yield was >95%, which was checked by ICP-OES (Varian 720-ES).

2.4. Mass spectrometry

Silicon isotope composition was measured on a Thermo Neptune multi-collector inductively coupled mass spectrometer (MC-ICP-MS) equipped with an H-skimmer cone and the newly developed Thermo Scientific® Jet-interface in high-resolution mode (m/Δm > 5000). The purified sample solutions were introduced into the plasma via a desolvation unit for dry plasma conditions (Apex, ESI®, no N$_2$ addition, no further membrane desolvation) equipped with a 120 μl/min nebulizer.

We used Mg doping combined with standard-sample-bracketing to correct for mass bias during measurements by using an exponential mass bias law (Cardinal et al., 2003). A magnesium solution was added to samples and standards to yield a final concentration of 1 ppm Mg. Sample solutions were diluted to 1 ppm Si concentration in 0.1 M HCl, which typically resulted in an intensity of ~15 V/ppm on ^{28}Si (using a 10^{11} Ω resistor).

Measurements were conducted on the interference-free low-mass side of the three Si isotopes. The most critical interference, caused by $^{14}N^{16}O$ on the ^{30}Si signal, is usually below 5 V which is resolvable from the ^{30}Si signal in the high-resolution mode used. Each sample and standard was measured at least 4 times during a sequence; each sample or standard was measured in dynamic mode for 30 cycles with an integration time for each cycle of 4 s for Si as well as for Mg with an idle time of 3 s after magnet switching. Pure 0.1 M HCl solutions were measured before and after each standard–sample–standard block and were used for on-peak zero correction. Typical intensities of ^{28}Si in blank solutions were below 5 mV. We report Si isotope data relative to the standard reference material NBS28 (quartz sand) in the delta notation according to Coplen (2011) as $\delta(^{29/28}Si)_{NBS28}$ and $\delta(^{30/28}Si)_{NBS28}$ expressed in per mill (‰) by multiplication of Eqs. (1) and (2) with a factor of 10^3:

$$\delta\left(^{29/28}\text{Si}\right)_{\text{NBS28}} = \left(\frac{\left(\frac{^{29}\text{Si}}{^{28}\text{Si}}\right)_{\text{sample}}}{\left(\frac{^{29}\text{Si}}{^{28}\text{Si}}\right)_{\text{NBS28}}} - 1\right) \qquad (1)$$

$$\delta\left(^{30/28}\text{Si}\right)_{\text{NBS28}} = \left(\frac{\left(\frac{^{30}\text{Si}}{^{28}\text{Si}}\right)_{\text{sample}}}{\left(\frac{^{30}\text{Si}}{^{28}\text{Si}}\right)_{\text{NBS28}}} - 1\right). \qquad (2)$$

All reported errors on delta values are the 95% confidence interval (CI) calculated according to Eq. (3) where $\overline{\delta(^{30/28}Si)_{NBS28}}$ is the mean of the measured delta values for the sample or standard (at least n = 4), t_{n-1} is a critical value from tables of the Student's t-law and SE is the standard error of the mean.

$$\text{CI} = \overline{\delta\left(^{30/28}\text{Si}\right)_{\text{NBS28}}} \pm t_{n-1} \times \text{SE} \qquad (3)$$

The well-defined Si isotope reference material BHVO-2 g, a basalt standard (measured over a 12 months period of analysis ; including several individual chemical separations as well as several digestions procedures; $\delta(^{30/28}\text{Si})_{\text{NBS28}} = -0.27 \pm 0.02; n = 73$), was usually measured as control standard during measured sequences.

2.5. Analytical tests

As it is mentioned in Section 2.1 the side product during monomeric silicic acid preparation using TEOS is ethanol. In a separate experiment using similar starting material (Oelze et al., unpublished) it has been
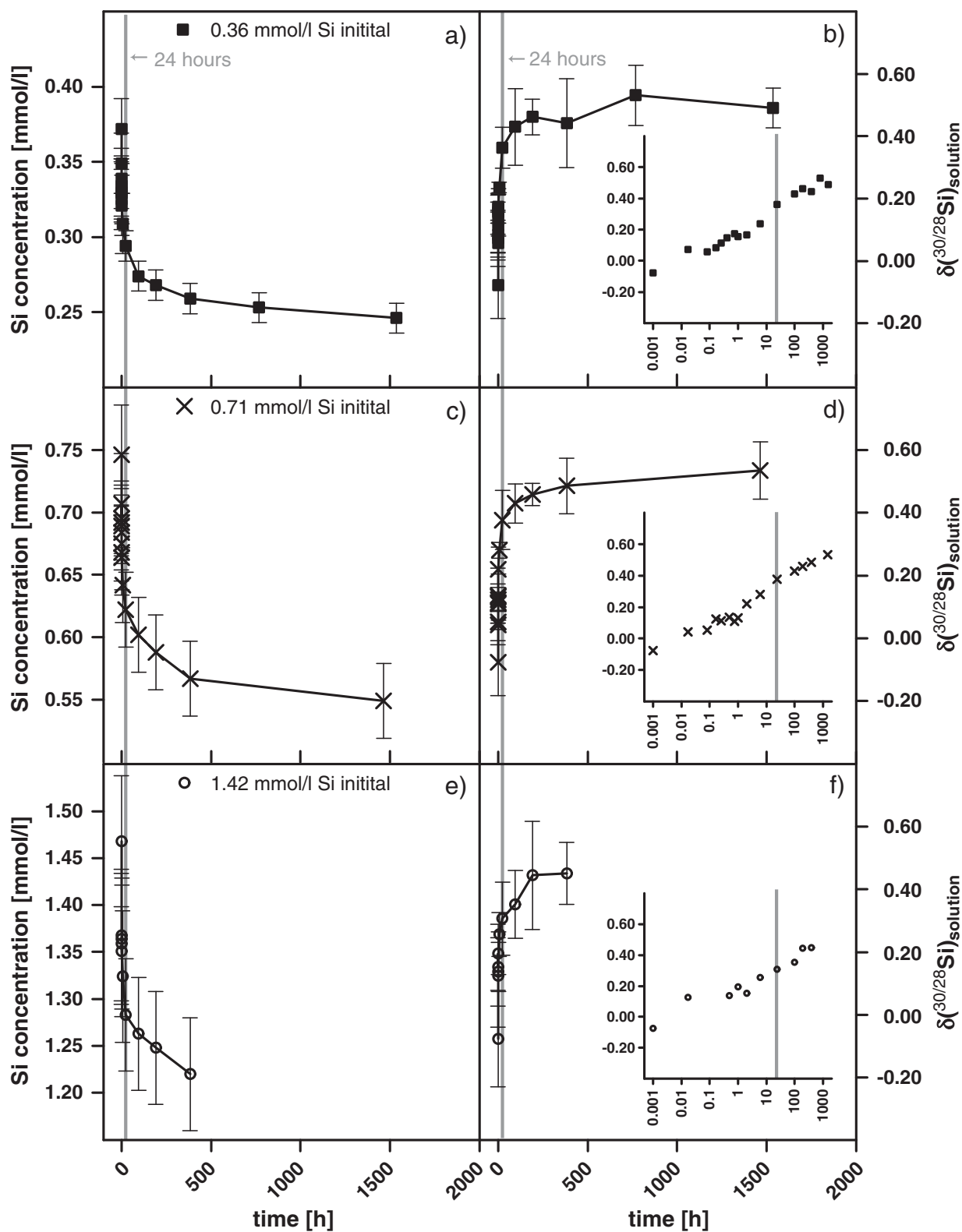
Fig. 1. Evolution of Si concentration (panels a, c and e) and $\delta(^{30/28}\text{Si})_{\text{solution}}$ (panels b, d and f) of the solution with time during adsorption experiments (30 g/l of gibbsite, pH 7.0). Squares, crosses and circles depict experiment with an initial Si concentration of 0.36, 0.71 and 1.42 mmol/l, respectively. Insets in panels b, d and f show the same isotopic datasets plotted vs. log time in hours.

tested whether the remaining ethanol in the prepared solutions induces analytical artifacts during the preparation and measurement of Si isotopes. Pairs of solutions and the formed solid counterparts were measured. Applying a mass balance approach showed that all fluid–solid pairs gave the isotopic composition of the starting solution. Hence no mass-spectrometric artifact was induced from the release of ethanol during preparation of Si-containing solutions using TEOS.

A known limitation of using the sample purification method of Georg et al. (2006b) is that anions present in the samples remain in the purified Si solutions. As the Si adsorption experiments were conducted in the presence of 0.1 M NaCl and further HCl has been used to adjust the pH, Cl^- anions might have been present after purification and potentially might have caused matrix effects as their amounts are different between sample and bracketing standards. Therefore we tested whether different amounts of Cl^- anions in sample and bracketing standard causes matrix effects by measuring a "Cl^- -doped" standard against "pure" bracketing standards. In the estimated range of different Cl^- anion concentrations (difference between "doped" and "pure" of up to 20%) no bias has been found.

3. Results

Si concentrations as well as $\delta(^{29/28}Si)_{solution}$ and $\delta(^{30/28}Si)_{solution}$ values are reported in Online Supplement Table A.1.

3.1. Evolution of Si concentration

During the adsorption experiments, a continuous decrease in Si concentration with time is observed (Fig. 1). In all experiments (0.36, 0.71 and 1.42 mmol/l Si starting concentration) the major change of Si

concentration occurs during the first 50 h, and subsequently the changes slow down continuously. Over 60% of the total adsorption takes place during the first 24 h. Si adsorption rates (Fig. 2) at the beginning of the experiments differ strongly between the conducted experiments. Adsorption rates for experiments with an initial Si concentration of 1.42 mmol/l are up to four times higher compared to solutions with an initial concentration of 0.36 mmol/l Si; the 0.71 mmol/l Si solution experiment yields intermediate adsorption rates. Using estimates from Karamalidis and Dzombak (2011) of 8–8.8 adsorption surface sites/nm² on gibbsite and the measured BET surface area of 1.18 m²/g a maximum possible amount of adsorbed Si of 440–484 μg/g (470–520 μmol Si total) can be calculated. As the maximum Si amounts adsorbed (defined by the equilibrium constant of the adsorption reaction) were ca. 130, 200, and 250 μmol for the 0.36, 0.71, and 1.42 mmol/l experiment, respectively, in all adsorption experiments an excess of free adsorption surface sites was still available at the end of the experiments.

3.2. Silicon isotopes

We report measured $\delta(^{30/28}Si)_{solution}$ solution values (measured relative to NBS28) throughout this section. All three adsorption experiments (with initial Si concentrations of 0.36, 0.71 and 1.42 mmol/l) display a similar evolution of their $\delta(^{30/28}Si)_{solution}$ values. With increasing experimental runtime or decreasing fraction of Si remaining in solution ($f_{solution}$), the dissolved Si becomes increasingly enriched in ^{30}Si, which results in higher $\delta(^{30/28}Si)_{solution}$ values (Fig. 3). The largest changes in $\delta(^{30/28}Si)_{solution}$ are observable during the first 24 h where also over 60% of the Si adsorption onto gibbsite takes place. After this initial period of rapid change in both Si concentration and $\delta(^{30/28}Si)_{solution}$, the change
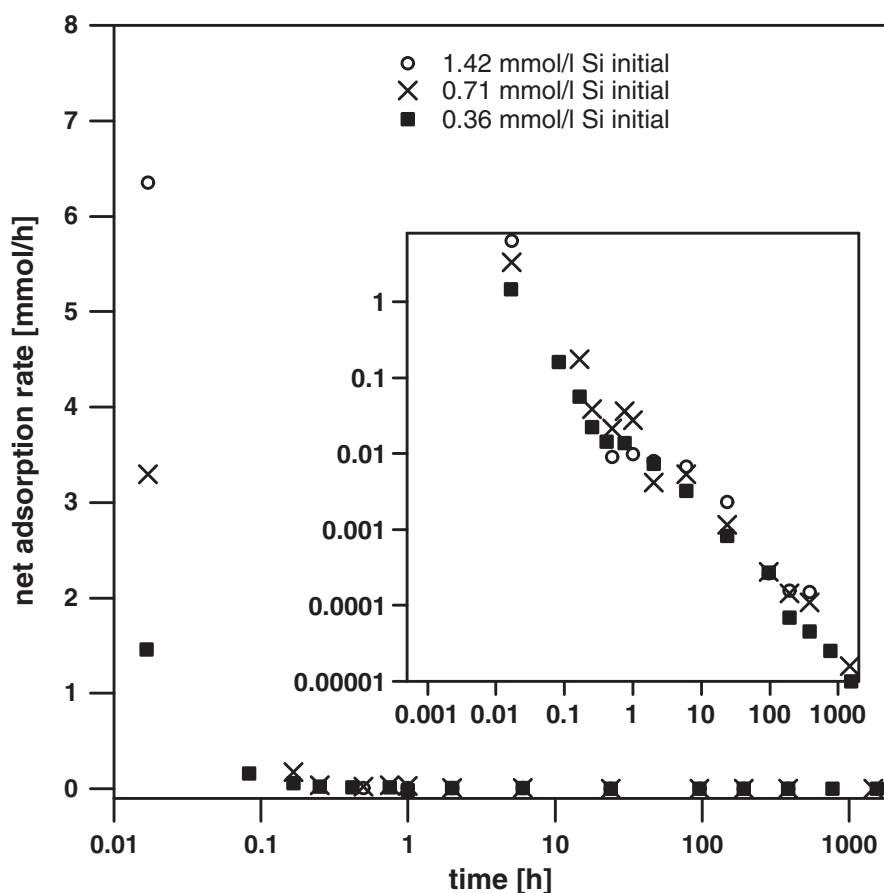
Fig. 2. The net adsorption rate vs. time in a semi-log diagram (inset log-log scale). Net adsorption rate dq/dt is calculated as the difference between the amount adsorbed in mmol $dq = q_{n+1} - q_n$ divided by the time elapsed in hours $dt = t_{n+1} - t_n$.
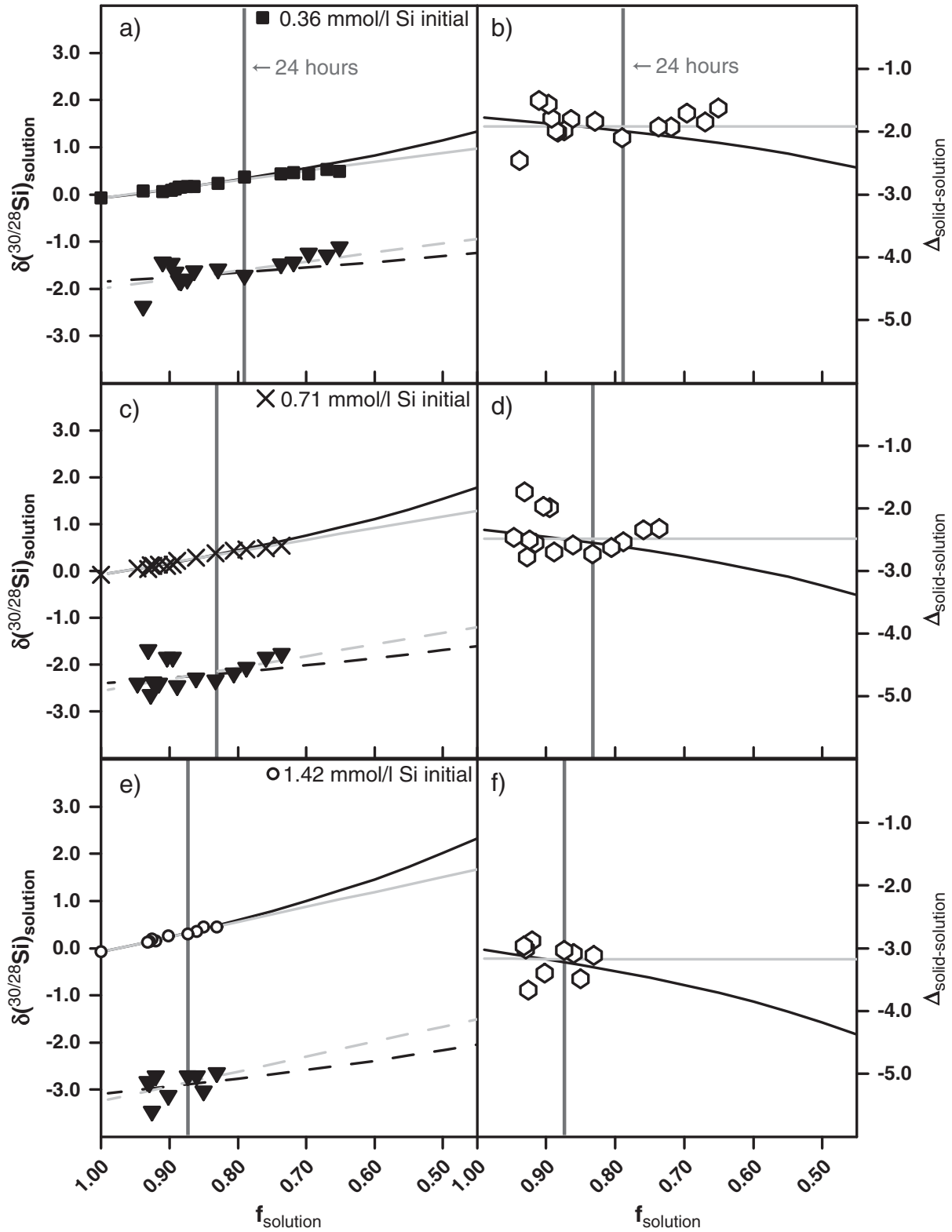
Fig. 3. The left panels (a, c and e) show the $\delta(^{30/28}Si)_{solution}$ evolution of the measured solution and the corresponding calculated $\delta(^{30/28}Si)_{adsorbed}$ of the solid in the adsorption experiments, as a function of the fraction of Si remaining in solution ($f_{solution}$). The open diamonds in the right panels (b, d and f), show the isotopic difference $\Delta(^{30/28}Si)_{solid - solution}$ between solid and solution as a function of the fraction of Si remaining in solution ($f_{solution}$). In the left panels, squares, crosses and circles depict experiments with initial Si concentrations of 0.36, 0.71 and 1.42 mmol/l, respectively. The triangles depict $\delta(^{30/28}Si)_{adsorbed}$ calculated for the corresponding Si adsorbed onto solids for each individual experiment. Regression lines for the experimental data (first 24 h) fitted according to the open-system mass balance approach (black lines; Eq. (4)) and for the closed-system approach (gray lines; Eq. (5)) are also shown (see Table 1 for obtained fractionation factors; error bars are smaller than symbol size).

in $\delta(^{30/28}Si)_{solution}$ is much slower. In fact in contrast to the continuously evolving Si concentrations $\delta(^{30/28}Si)_{solution}$ values are almost constant. Finally a maximum $\delta(^{30/28}Si)_{solution}$ value is reached where Si

concentration and $\delta(^{30/28}Si)_{solution}$ remain virtually constant (see Online Supplement Table A.1). We only used the data of the first 24 h to determine an apparent isotope fractionation factor $\alpha_{adsorbed/solution}$ for each of

Table 1

Resulting $\alpha^{30/28}Si_{adsorbed/solution}$ and $10^3 \ln \alpha^{30/28}Si_{adsorbed/solution}$ values using adsorption data of the first 24 h. To determine isotope fraction factors an open-system and a closed-system mass balance model has been applied to the experimental data. To fit the data we used the nlme-package (Pinheiro et al., 2014) in R (R Core Team, 2014). We report the calculated standard error (SE) of $\alpha^{30/28}Si$ and the standard error of the residuals (RMSD) calculated for each experiment.

Experiment	$\alpha^{30/28}Si$	$10^3 \ln \alpha^{30/28}Si$	RMSD
"Open-system" mass balance			
0.36 mmol/l Si initial	0.998222 ± 0.000050	-1.779 ± 0.050	0.022
0.71 mmol/l Si initial	0.997669 ± 0.000088	-2.334 ± 0.088	0.030
1.42 mmol/l Si initial	0.996986 ± 0.000102	-3.019 ± 0.102	0.023
"Closed-system" mass balance			
0.36 mmol/l Si initial	0.998071 ± 0.000060	-1.931 ± 0.060	0.025
0.71 mmol/l Si initial	0.997516 ± 0.000100	-2.487 ± 0.100	0.033
1.42 mmol/l Si initial	0.996827 ± 0.000103	-3.178 ± 0.103	0.022

the experiments. We define $\alpha_{adsorbed/solution}$ ($\alpha_{adsorbed/solution} = (^{30}Si/^{28}Si)_{adsorbed}/(^{30}Si/^{28}Si)_{solution}$) as the isotope fractionation factor between adsorbed Si and dissolved Si remaining in solution. However, the composition of Si adsorbed onto gibbsite $\delta(^{30/28}Si)_{adsorbed}$ was calculated by mass balance, as the gibbsite remained in the experimental containers throughout the experiment. An "open-system" (Rayleigh mass balance) and a "closed-system" mass balance approach were applied to the data (Johnson et al., 2004). An "open-system" mass balance approach assumes that the product (here adsorbed Si) does not remain in contact with the starting material (here dissolved Si) after formation. In this case the evolution of dissolved Si isotope composition is given by:

$$\frac{\left(1000 + \delta\left(^{30/28}Si\right)_{solution}\right)}{\left(1000 + \delta\left(^{30/28}Si\right)_{solution-initial}\right)} = f_{solution}^{\left(\alpha_{adsorbed/solution}-1\right)}. \tag{4}$$

In contrast, a "closed-system" approach assumes complete isotope exchange during removal of dissolved Si, leading to:

$$\delta\left(^{30/28}Si\right)_{solid} = \delta\left(^{30/28}Si\right)_{solution-initial} + 1000 * f * \left(\alpha_{adsorbed/solution}-1\right). \tag{5}$$

As $f_{solution}$ did not extend to values lower than 0.6, our data does not allow one to identify whether the experiments follow "open-system" or "closed-system" behavior. We return to this question in Section 4.1. Here we apply both types of mass balance models to our data, and obtain a reasonable fit for each experiment. Three distinct isotope fractionation factors are obtained for both mass balance approaches (see Fig. 3 and Table 1).

4. Discussion

4.1. Si isotope fractionation during Si adsorption

During our adsorption experiments significant changes of Si concentration are associated with changes in the $\delta(^{30/28}Si)_{solution}$ values, where light isotopes are preferentially adsorbed onto the gibbsite surface. We further observe a higher Si isotope fractionation between adsorbed and dissolved Si the higher the initial Si concentration is.

We first explore whether isotope fractionation found between Si adsorbed onto solids and Si remaining in solution follows a "closed-system" behavior (Johnson et al., 2004). In our experiments the range of Si fractions remaining in solution (0.7 to 1.0) experienced does not allow one to distinguish the "closed" system behavior from the "open" system case. Therefore, the observed pattern is compatible with a "closed-system" behavior and hence continuous contact and exchange between solids and solution. Such re-equilibration has been shown to be characterized by equilibrium isotope fractionation in previous adsorption experiments (Juillot et al., 2008; Wasylenki et al., 2008, 2011). However, we can rule out equilibrium isotope fractionation as the adsorption rate is high from hours 0 to 400, which argues against attainment
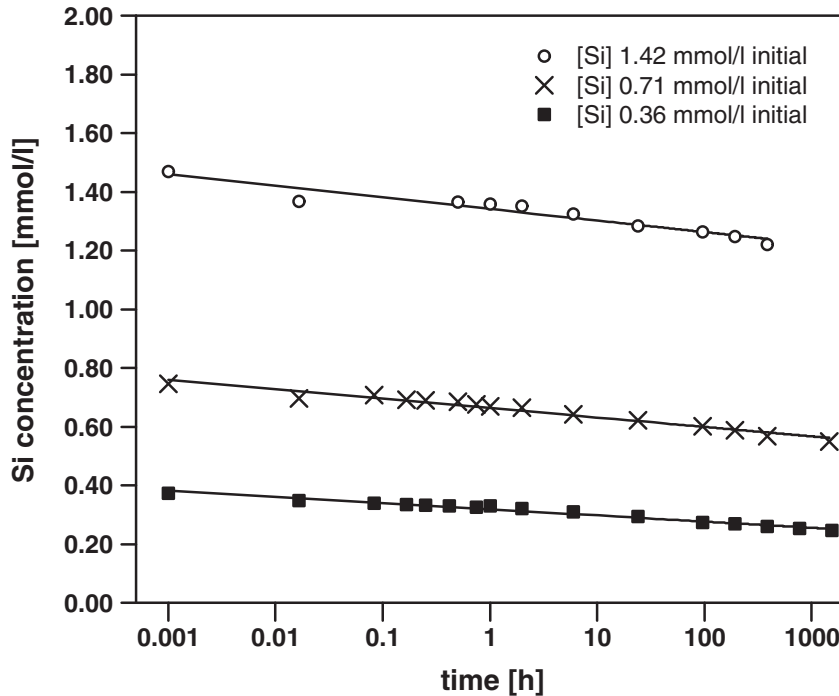
Fig. 4. Si concentration vs. time (on log scale), where the slopes denotes the overall adsorption rate (Eq. (6)) Squares depict the experiment with an initial Si concentration of 0.36 mmol/l, crosses depict experiment with 0.71 mmol/l and circles the experiment with 1.42 mmol/l initial Si concentration. Adsorption experiments with high initial Si concentration show steeper slopes than lower Si initial concentration experiments, which means the higher the Si initial concentration the higher the adsorption rate.

of chemical equilibrium — a prerequisite for isotopic equilibrium. Therefore we proceed to discuss our results in terms of the "open-system" behavior.

We next discuss the prevailing mechanism of adsorption of light isotopes onto the gibbsite surfaces. Any transport-induced isotope effect (e.g. isotope fractionation of Si through diffusion) can be ruled out, as the experimental solutions were constantly heavily stirred or shaken. Hence the occurrence of Si isotope fractionation in our experiments can be explained by the adsorption process being "reaction-limited" i.e. the fractionation depends on the kinetics of the adsorption reaction when an activation energy barrier E_a during formation or breaking of bonds has to be overstepped. The Arrhenius equation demands that reactions of light isotopes are preferred over those of heavy isotopes (Bigeleisen, 1965). Yet even this activation energy barrier model does not explain the dependence of $\alpha_{adsorbed/solution}$ on the initial Si concentration. As also Si adsorption rates differ significantly between our experiments, we next evaluate how reaction kinetics might affect isotope fractionation.

4.2. Kinetics of Si adsorption

Adsorption reaction kinetics of Si onto gibbsite was often described as a first-order reaction, at least for some parts of the reaction (Hingston and Raupach, 1967; Adu-Wusu and Wilcox, 1991; Dietzel, 2002). An attempt to explain the overall adsorption reaction with simple kinetic rate laws (first-order, second-order or first-order forward and backward reaction, see Online Supplement C) fails. The evolution of Si concentration follows a linear trend in a semi-log diagram (Fig. 4) and therefore we apply the empirical equation:

$$[Si] = a \times \log(time) - b. \tag{6}$$

In such a diagram the slope a is a coefficient describing the relative adsorption rate. For each adsorption experiment, the data describe a straight line but different slopes are obtained. This dependence can be interpreted to mean that distinct initial Si concentrations result in different Si adsorption rates. The higher the initial Si concentration, the faster the adsorption (see Fig. 4).

When for all three adsorption experiments the apparent Si isotope fractionation factor (derived for the first 24 h from the open-system mass balance model; see Table 1) is plotted against the slope obtained from the empirical logarithmic relationship (Eq. (6)) a strong linear relationship is obtained (see Fig. 5). With increasing adsorption rate the determined fractionation factors decrease. Hence the Si isotope fractionation depends on adsorption rate.

4.3. The change of the isotope fractionation regime

Two explanations can be invoked to explain the rate dependence of isotope fractionation factors between the three experiments. Given that the isotope-specific energy barrier of a chemical pathway does not depend on adsorption rate, the first explanation is that reactions pathways differ between experiments. The second explanation is that a significant relative rate of a back reaction and the associated isotope fractionation affects the experiments, differs between the experiments. A framework that relates isotope fractionation to the ratio of backward to forward reaction rate has been developed by DePaolo (2011). This conceptual model is based on simple definitions of a forward reaction rate R_f (formation of new phases; here Si adsorption onto gibbsite), a backward reaction rate R_b (dissolution of newly formed phases; here Si desorption from gibbsite) and the net reaction rate R_p ($R_p = R_f - R_b$). The forward and backward rates are associated with distinct kinetic isotope fractionation factors (α_f and α_b, respectively). An apparent fractionation factor α_p arises from the R_p/R_b ratio (see Eq. 11 in DePaolo, 2011). The overall prediction is that if the net adsorption rate R_p is much larger than the backward rate R_b, the apparent isotope fractionation will be kinetically dominated (favoring light isotopes). By contrast if R_p is much smaller than R_b, the system reaches isotopic fractionation at equilibrium.
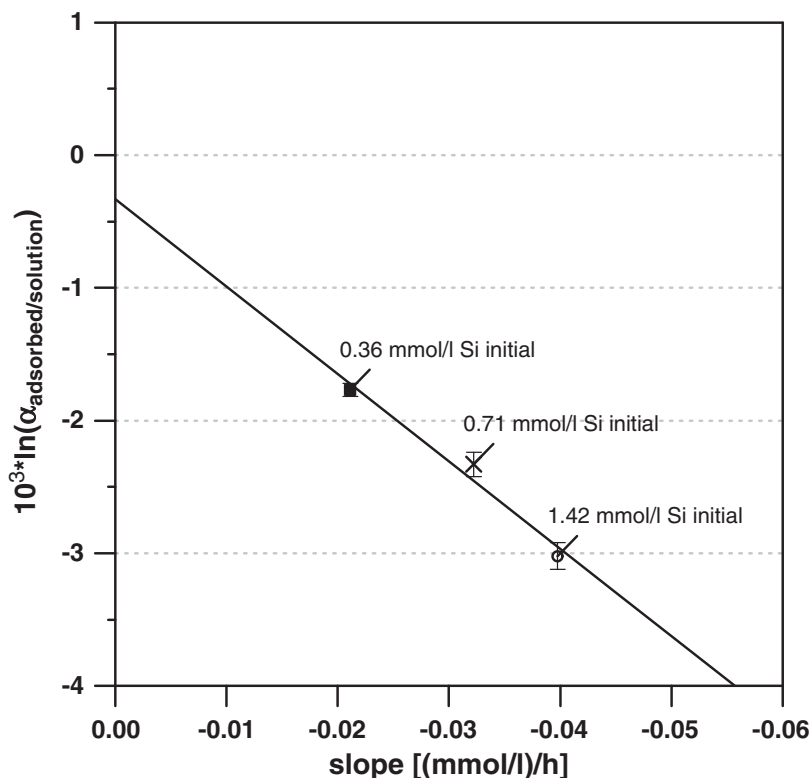
Fig. 5. Fractionation factors as $10^3 \ln(\alpha_{adsorbed/solution})$ deduced from applying an open-system mass balance to the first 24 h of the individual adsorption experiments (Table 1) vs. the slope derived from applying the empirical logarithmic relationship (Eq. (6)).

While at intermediate regimes α_p depends on the values of α_f, α_b and R_p/R_b. On the low and on the high end of the R_p/R_b axis (Fig. 6) plateaus in α_p emerge. We can evaluate whether the dependence of the fractionation factor on adsorption rate can be interpreted within this framework.

First, for a given experiment, net adsorption rates decrease abruptly over the first 24 h, hence it is most likely that the R_p/R_b ratio changes. However, $\alpha^{30/28}Si_{adsorbed/solution}$ (α_p in DePaolo's (2011) terminology) remains constant. This means that the early stage of our experiments cannot be interpreted as being located at intermediate R_p/R_b values where α_p is expected to be strongly dependent on adsorption rate (Fig. 6). Second, as there is net adsorption during this early stage, the experiments cannot be interpreted as operating near chemical and isotopic equilibrium, hence they are likely not located on the low end of the R_p/R_b axis (Fig. 6). Therefore, for the first 24 h in each experiment, the constant α_p value while R_p/R_b ratios change means that the experiments are located, on the "kinetic plateau". There, at the high end of R_p/R_b values, $\alpha_p \sim \alpha_f$. The difference between the apparent isotope fractionation factors then reflects different values of the kinetic isotope fractionation factors associated with the forward reaction.

We therefore conclude that the observed dependence of Si isotope fractionation on the initial Si concentration can only be explained within the DePaolo framework if α_f values differ between the three experiments (Fig. 6).

After 24 h $\delta(^{30/28}Si)_{solution}$ and hence $\alpha^{30/28}Si_{adsorbed/solution}$ changes. We can interpret this second stage of the experiments within the DePaolo framework as only then R_b increases at the cost of R_f and hence α_p departs from the kinetic plateau and evolves towards equilibrium. We can estimate the equilibrium isotope fractionation factor from the linear correlation of the overall net adsorption rate and the determined closed-system isotope fractionation factors (see Fig. 5). Extrapolated to a zero net adsorption rate, an equilibrium isotope fractionation factor of $\alpha^{30/28}Si_{adsorbed/solution} = 0.9997$ ($10^3 \ln \alpha^{30/28}Si_{adsorbed/solution} = -0.3‰$) results.

That α_f values depend on Si concentrations is an unexpected conclusion that warrants an explanation. At the early stage of this finding we can only speculate on its cause. We can exclude that our high-concentration experiments were limited in adsorption sites, such that the removal mechanism shifted from one of adsorption to one for example of precipitation (see Section 3.1). The most likely process is hence adsorption onto monolayers in all three experiments. It is conceivable that a shift in surface complexation occurs with increasing Si concentration and that different complexes differ by the strength of their adsorption site and are hence associated with different α_f values (Lemarchand et al., 2007). However, this assumption is not supported by surface complexation models which are able to reconcile the evolution of Si adsorption onto gibbsite using only one surface complex (Karamalidis and Dzombak, 2011). We note that the poor fit and the small amount of usable data of that study does not allow one to fully rule out this explanation either. A second possible explanation is the polymerization of silicic acid at the gibbsite surface and therefore the formation of $Si–O–Si$ bonds that are probably associated with different isotope fractionation factors. Yokoyama et al. (1982) reported the polymerization of Si at the surface of Al-hydroxides but only for much higher concentrations of dissolved Si. However, in a precipitation experiment Oelze et al. (unpublished) observed a fractionation factor $\alpha_p = 1$ for polymerization of silicic acid. Therefore further studies on the exact adsorption process of Si onto Al-hydroxides are needed to resolves this issue.
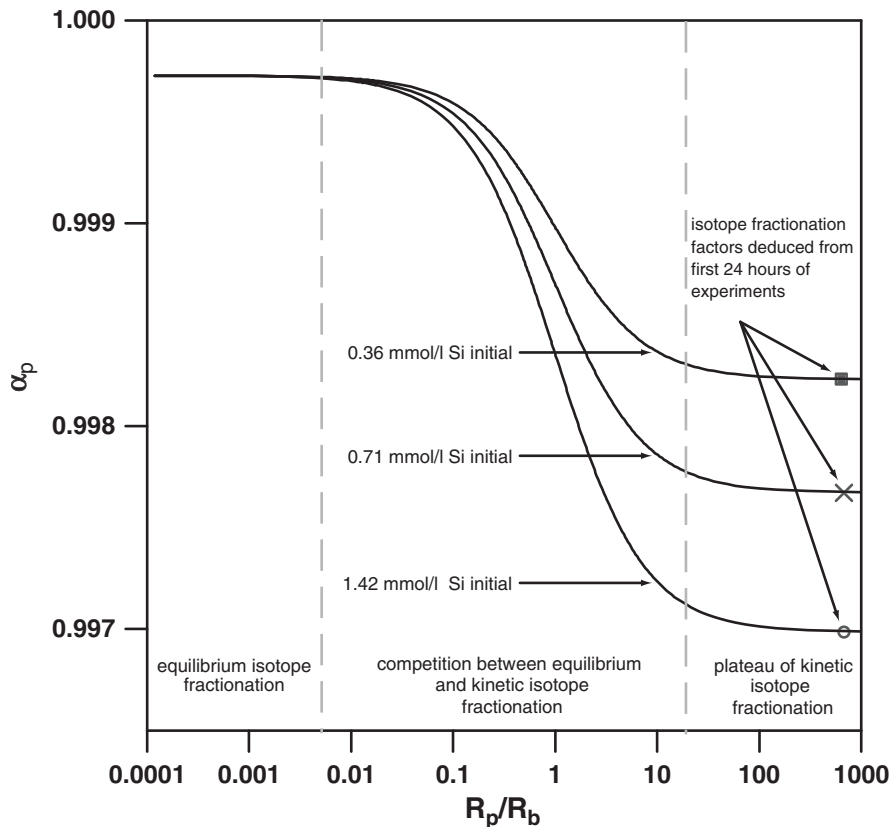
Fig. 6. Model curve of α_p vs. R_p/R_b using the "DePaolo-Model" (black lines) as a function of R_p/R_b. The α_f values for different initial Si concentrations were deduced from the calculated closed-system isotope fractionation factor for the first 24 h of the individual experiments (see Fig. 2 and Table 1). The isotope fractionation factor at equilibrium is inferred from the linear correlation of the overall net adsorption rate and the closed-system isotope fractionation factors (see Fig. 4). For a zero net adsorption rate the equilibrium isotope fractionation factor results to $\alpha_{eq} = 0.9997$.

4.4. Si adsorption in natural systems

Si adsorption onto gibbsite (this study) and onto Fe-oxides (Delstanche et al., 2009) both favor light Si isotopes while the remaining solution accumulates the heavy Si isotopes. Delstanche et al. (2009) computed fractionation factors for Si adsorption onto Fe-oxides ($10^3 \ln \alpha^{30/28}Si_{ferrihydite/solution} = -1.05‰$ and $10^3 \ln \alpha^{30/28}Si_{goethite/solution} = -1.56‰$). These fractionation factors were shown to be independent of Si concentration (Delstanche et al., 2009). There are two ways to explain the contrasting behavior of Si isotope between these two series of experiments: (i) Delstanche et al. (2009) propose that the Si isotope fractionation during adsorption onto Fe-oxides is caused by the formation of a Fe oxide-monosilicate bi-dendate inner surface complex. The apparent isotope fractionation factor during Si adsorption is expected to depend in particular on the kinetics of the formation of this distinct surface complex. The formation rate of this surface complex might be independent of Si concentration and thus no dependence of Si concentration and isotope fractionation would be observed. (ii) We can also use the "DePaolo-Model" (DePaolo, 2011) to explain this behavior. If we assume that the net adsorption rate is much higher than the backward rate, the resulting α_p is firmly located within the kinetically dominated regime and is thus independent of small changes of R_p/R_b (see Fig. 6). Both explanations are conceivable.

4.5. Comparison to adsorption of transition metals

The isotopic behavior of Si during adsorption differs fundamentally from that observed in studies of transition metals. The adsorption of molybdenum onto Mn-oxide surfaces was shown to attain equilibrium within <10 h (Wasylenki et al., 2008). Adsorption of zinc onto ferryhydrite and goethite surfaces attained isotopic equilibrium after <20 h (Juillot et al., 2008). Adsorption of ferrous iron to surfaces of goethite, quartz, goethite-loaded quartz, and aluminium oxide resulted in attainment of equilibrium within <72 h (Mikutta et al., 2008). Given such rapid equilibration time scales and the observed "closed-system" behavior, in natural environmental systems such transition metal results can be interpreted in terms of equilibrium isotope fractionation. The opposite is observed for silica. The strong kinetic isotope fractionation accompanying Si adsorption and its sluggish re-equilibration, even after several months of experimental runtime, makes it likely that natural systems are dominated by kinetic isotope effects. This conclusion bears important implications for weathering systems that we explore in the next section.

4.6. Implications for silicate weathering environments

Many recent studies attribute the heavy Si isotopic signature of soil and stream water to the formation of secondary minerals containing the complementary reservoir of light Si isotopes (Douthitt, 1982; de La Rocha et al., 2000; Basile-Doelsch et al., 2005; Ziegler et al., 2005a; Basile-Doelsch, 2006; Georg et al., 2006a, 2009; Opfergelt et al., 2011). However, the formation of secondary silicate minerals is sufficiently slow so that equilibrium isotope fractionation can be expected (Iler, 1979; Sposito, 1996). The Si isotope fractionation factors inferred from ab initio calculations (Méheut et al., 2009) and experimental studies show that ^{28}Si will not be preferentially incorporated into the clay fraction if dissolved Si and crystalline silicates are in isotopic equilibrium. How then can the enrichment of ^{28}Si in clays found in weathering systems be explained?

With increasing age and/or stage of silicate weathering the composition of secondary solids changes from one dominated by amorphous solids to one dominated by crystalline clay minerals (Ziegler et al., 2003; Joussein et al., 2005). For instance, a known transformation path is the reaction of plagioclase to amorphous alumosilicates such as allophane, subsequently e.g. to halloysite, and finally to clay minerals such as kaolinite. It is indeed more likely that kaolinite is formed via

thermodynamically less stable phases which act as precursors such as allophane and halloysite (Steefel and Van Cappellen, 1990).

In any case, the first step is the release of Al and Si from primary minerals such as plagioclase. At pH values between 5 and 7 and at the low dissolved organic carbon concentrations typically prevailing in soils or in interstitial solutions, the solubility of $Al(OH)_3$ is extremely low (Sposito, 1996). Accordingly, Al precipitates as amorphous $Al(OH)_3$ or as crystalline solids such as gibbsite. The affinity of Si to adsorb onto these precipitated Al-hydroxides is high (Hingston and Raupach, 1967; Adu-Wusu and Wilcox, 1991; Dietzel, 2002). As we have shown in this study, Si adsorption onto Al-hydroxides is associated with rather strong Si isotope fractionation, favoring light Si isotopes adsorbed onto the solid surface. In the next step, amorphous alumosilicates like siliceous gels or colloids such as hydroxyaluminosilicate (HAS) are formed. Accordingly, Strekopytov et al. (2006) suggested that, for HAS formation, the reaction of Si with Al-hydroxides is a prerequisite. Such amorphous Al–Si phases can be re-arranged to structures with higher degrees of order, similar to allophane or imogolite (Sposito, 1996; Doucet et al., 2001). If the transformation from amorphous Al–Si phases without any short range order to phases with distinct short range order like HAS or allophane takes place without substantial exchange of Si, the Si isotope signature of HAS/allophane will be inherited from the initial fast adsorption process of Si. With ongoing weathering, the halloysite content in the soil decreases, whereas the kaolinite content increases (Papoulis et al., 2004). As halloysite has the same structure and chemical compositions as kaolinite except for the higher water content in halloysite (Joussein et al., 2005), we can assume that during the transformation of halloysite to kaolinite no shift in Si isotope composition occurs, as Si will be neither lost nor added. Therefore, we suggest that the Si isotopic signature of crystalline clay minerals, such as kaolinite, is inherited from the kinetically-dominated process occurring during adsorption of Si onto a previously formed amorphous Al-hydroxide.

Our model of inherited isotope signals has important implications for interpreting element cycles in the different weathering regimes observed at the Earth surface. In the kinetically limited weathering regime (where supply into and erosion from the weathering zone is so fast that not all primary minerals are dissolved (West et al., 2005; Ferrier and Kirchner, 2008; Dixon et al., 2012) and solutions are at equilibrium concentrations (Maher, 2011)), the Si isotopic signature of soil or stream water will inevitably show heavy Si isotopic values, as in such regimes only fast processes like adsorption of Si occur and no light Si will be released from secondary minerals due to their short residence time in the weathering zone. In the supply-limited weathering regime (where supply and erosion of primary minerals is so slow that most primary minerals are exhausted (West et al., 2005; Ferrier and Kirchner, 2008; Dixon et al., 2012) and solutions are diluted with respect to equilibrium concentrations (Maher, 2011)), the Si isotopic signature of the soil or stream water will be characterized by the degree of weathering, ranging from heavy Si isotopic signatures, where kinetically dominated Si adsorption is the major process, to light Si isotopic signatures where the system is governed by dissolution of clay minerals. This has been already shown for tropical supply-limited settings in the black-water rivers of the Amazon and Congo basin (Cardinal et al., 2010; Hughes et al., 2013). Where erosion rates of secondary minerals are low, it is also conceivable that adsorption of Si and dissolution of secondary minerals are balanced out which results then in an isotopic signature of soil and stream water indistinguishable from the parent material. The dissolution of previously formed secondary precipitates dominates and these minerals release their inherited light Si (Bouchez et al., 2013). Such temporal evolution has been observed from chronosequences in Hawaii (Ziegler et al., 2005a). These authors measured the isotopic signature of the soil solutions and observed an enrichment of heavy Si in solution with increasing age of the soil. In analogy, Opfergelt et al. (2011) clearly showed from allophane sequences in volcanic soils that the more weathered the soil, the older the allophane and the lighter the Si isotope signature is.

5. Summary

The adsorption of monomeric silicic acid onto gibbsite is accompanied by a significant kinetic Si isotope fractionation. In all adsorption experiments, light Si isotopes are preferentially adsorbed. By applying a closed-system mass balance model we calculate Si isotope fractionation factors that are dependent on the initial Si concentration. High initial Si concentrations result in a strong kinetic Si isotope fractionation during adsorption. This initial kinetic signature does begin to re-equilibrate only after ca. 2 months. With this sluggish behavior Si behaves fundamentally different from transition metals (e.g. Fe, Mo, Zn) that equilibrate isotopically within hours.

Application of the mass balance model of DePaolo (2011) requires the assumption of different isotope fractionation factors (α_f) associated with the forward reaction at different initial Si concentrations, rather than changes in forward to backward reaction rate. A minor shift in isotope ratios after 24 h of Si adsorption is explained by a change in the isotope fractionation regime from kinetically dominated to dominated by equilibrium isotope fractionation. This behavior is compatible with a change from high net adsorption rates to low net adsorption rates (almost constant Si concentration at the end of experiments).

Our findings have major relevance for explaining Si isotope systematics during silicate weathering. We hypothesize that the light Si isotopes signatures commonly found in secondary siliceous minerals and amorphous solids are obtained from adsorption of Si onto Al-hydroxides during the early stages of weathering. When these amorphous phases slowly age to ordered structures and clay minerals, the low isotope ratio is passed on from the amorphous precursors. The light isotope composition found in clays is therefore inherited from the early stages of primary mineral decomposition.

Acknowledgments

Appendix A. Supplementary data

Supplementary data to this article can be found online at http://dx.doi.org/10.1016/j.chemgeo.2014.04.027.

References

Adu-Wusu, K., Wilcox, W.R., 1991. Kinetics of silicate reaction with gibbsite. J. Colloid Interface Sci. 143, 127–138.

Basile-Doelsch, I., 2006. Si stable isotopes in the Earth's surface: a review. J. Geochem. Explor. 88, 252–256.

Basile-Doelsch, I., Meunier, J.D., Parron, C., 2005. Another continental pool in the terrestrial silicon cycle. Nature 433, 399–402.

Bern, C.R., Brzezinski, M.A., Beucher, C., Ziegler, K., Chadwick, O.A., 2010. Weathering, dust, and biocycling effects on soil silicon isotope ratios. Geochim. Cosmochim. Acta 74, 876–889.

Bigeleisen, J., 1965. Chemistry of isotopes: isotope chemistry has opened new areas of chemical physics, geochemistry, and molecular biology. Science 147, 463–471.

Bouchez, J., von Blanckenburg, F., Schuessler, J.A., 2013. Modeling novel stable isotope ratios in the weathering zone. Am. J. Sci. 313, 267–308.

Cardinal, D., Alleman, L., de Jong, J., Ziegler, K., Andre, L., 2003. Isotopic composition of silicon measured by multicollector plasma source mass spectrometry in dry plasma mode. J. Anal. At. Spectrom. 18, 213–218.

Cardinal, D., Gaillardet, J., Hughes, H.J., Opfergelt, S., Andre, L., 2010. Contrasting silicon isotope signatures in rivers from the Congo Basin and the specific behaviour of organic-rich waters. Geophys. Res. Lett. 37, L12403.

Coplen, T.B., 2011. Guidelines and recommended terms for expression of stable-isotope-ratio and gas-ratio measurement results. Rapid Commun. Mass Spectrom. 25, 2538–2560.

de La Rocha, C.L., Brzezinski, M.A., DeNiro, M.J., 2000. A first look at the distribution of the stable isotopes of silicon in natural waters. Geochim. Cosmochim. Acta 64, 2467–2477.

Delstanche, S., Opfergelt, S., Cardinal, D., Elsass, F., Elsass, F., André, L., Delvaux, B., 2009. Silicon isotopic fractionation during adsorption of aqueous monosilicic acid onto iron oxide. Geochim. Cosmochim. Acta 73, 923–934.

DePaolo, D.J., 2011. Surface kinetic model for isotopic and trace element fractionation during precipitation of calcite from aqueous solutions. Geochim. Cosmochim. Acta 75, 1039–1056.

Dietzel, M., 1993. Depolymerisation von hochpolymerer Kieselsäure in wässriger Lösung. (Ph.D. thesis) , University Göttingen, Göttingen.

Dietzel, M., 2000. Dissolution of silicates and the stability of polysilicic acid. Geochim. Cosmochim. Acta 64, 3275–3281.

Dietzel, M., 2002. Interaction of polysilicic and monosilicic acid with mineral surfaces. Water Science and Technology Library. Springer, Netherlands, pp. 207–235.

Dietzel, M., Böhme, G., 1997. Adsorption and stability of polymeric silica. Chem. Erde 57, 189–203.

Dixon, J.L., Hartshorn, A.S., Heimsath, A.M., DiBiase, R.A., Whipple, K.X., 2012. Chemical weathering response to tectonic forcing: a soils perspective from the San Gabriel Mountains, California. Earth Planet. Sci. Lett. 323, 40–49.

Doucet, F., Rotov, M., Exley, C., 2001. Direct and indirect identification of the formation of hydroxyaluminosilicates in acidic solutions. J. Inorg. Biochem. 87, 71–79.

Douthitt, C.B., 1982. The geochemistry of the stable isotopes of silicon. Geochim. Cosmochim. Acta 46, 1449–1458.

Ferrier, K., Kirchner, J., 2008. Effects of physical erosion on chemical denudation rates: a numerical modeling study of soil-mantled hillslopes. Earth Planet. Sci. Lett. 272, 591–599.

Georg, R.B., Reynolds, B.C., Frank, M., Halliday, A.N., 2006a. Mechanisms controlling the silicon isotopic compositions of river waters. Earth Planet. Sci. Lett. 249, 290–306.

Georg, R.B., Reynolds, B.C., Frank, M., Halliday, A.N., 2006b. New sample preparation techniques for the determination of Si isotopic compositions using MC-ICPMS. Chem. Geol. 235, 95–104.

Georg, R.B., Reynolds, B.C., West, A.J., Burton, K.W., Halliday, A.N., 2007. Silicon isotope variations accompanying basalt weathering in Iceland. Earth Planet. Sci. Lett. 261, 476–490.

Georg, R.B., Zhu, C., Reynolds, B.C., Halliday, A.N., 2009. Stable silicon isotopes of groundwater, feldspars, and clay coatings in the Navajo Sandstone aquifer, Black Mesa, Arizona, USA. Geochim. Cosmochim. Acta 73, 2229–2241.

Gunnarsson, I., Arnorsson, S., 2000. Amorphous silica solubility and the thermodynamic properties of H_4SiO_4 degrees in the range of 0 degrees to 350 degrees C at P-sat. Geochim. Cosmochim. Acta 64, 2295–2307.

Hingston, F., Raupach, M., 1967. The reaction between monosilicic acid and aluminium hydroxide. I. Kinetics of adsorption of silicic acid by aluminium hydroxide. Aust. J. Soil Res. 5, 295–309.

Hughes, H.J., Sondag, F., Santos, R.V., André, L., Cardinal, D., 2013. The riverine silicon isotope composition of the Amazon Basin. Geochim. Cosmochim. Acta 121, 637–651.

Iler, R.K., 1979. The Chemistry of Silica: Solubility, Polymerization, Colloid and Surface Properties, and Biochemistry, John Wiley & Sons, Inc., New York.

Iler, R.K., 1982. Colloidal components in solutions of sodium silicate. Soluble Silicates. American Chemical Society, pp. 95–114.

Johnson, C.M., Beard, B.L., Albarede, F., 2004. Overview and general concepts. Rev. Mineral. Geochem. 55, 1–24.

Joussein, E., Petit, S., Churchman, J., Theng, B., Righi, D., Delvaux, B., 2005. Halloysite clay minerals — a review. Clay Miner. 40, 383–426.

Juillot, F., Maréchal, C., Ponthieu, m., Cacaly, S., Morin, G., Benedetti, M., Hazemann, J.L., Proux, O., Guyot, F., 2008. Zn isotopic fractionation caused by sorption on goethite and 2-Lines ferrihydrite. Geochim. Cosmochim. Acta 72, 4886–4900.

Karamalidis, A.K., Dzombak, D.A., 2011. Surface Complexation Modeling: Gibbsite, John Wiley & Sons, Inc., Hoboken, New Jersey.

Lemarchand, E., Schott, J., Gaillardet, J., 2007. How surface complexes impact boron isotope fractionation: evidence from Fe and Mn oxides sorption experiments. Earth Planet. Sci. Lett. 260, 277–296.

Maher, K., 2011. The role of fluid residence time and topographic scales in determining chemical fluxes from landscapes. Earth Planet. Sci. Lett. 312, 48–58.

Méheut, M., Lazzeri, M., Balan, E., Mauri, F., 2009. Structural control over equilibrium silicon and oxygen isotopic fractionation: A first-principles density-functional theory study. Chem. Geol. 258, 28–37.

Mikutta, C., Wiederhold, J.G., Hofstetter, T.B., Cirpka, O.A., Bourdon, B., von Gunten, U., 2008. Iron isotope fractionation during Fe(II) sorption to mineral surfaces. Geochim. Cosmochim. Acta 72, A627.

Opfergelt, S., de Bournonville, G., Cardinal, D., 2009. Impact of soil weathering degree on silicon isotopic fractionation during adsorption onto iron oxides in basaltic ash soils, Cameroon. Geochim. Cosmochim. Acta 73, 7226–7240.

Opfergelt, S., Georg, R.B., Burton, K.W., Guicharnaud, R., Siebert, C., Gislason, S.R., Halliday, A.N., 2011. Silicon isotopes in allophane as a proxy for mineral formation in volcanic soils. Appl. Geochem. 26, S115–S118.

Papoulis, D., Tsolis-Katagas, P., Katagas, C., 2004. Progressive stages in the formation of kaolin minerals of different morphologies in the weathering of plagioclase. Clay Clay Miner. 52, 275–286.

Pinheiro, J., Bates, D., DebRoy, S., Sarkar, D., R Core Team, 2014. nlme: Linear and Nonlinear Mixed Effects Models.

R Core Team, 2014. R: A Language and Environment for Statistical Computing, R Foundation for Statistical Computing, Vienna, Austria.

Sposito, G., 1996. The Environmental Chemistry of Aluminum, CRC Press.

Steefel, C.I., Van Cappellen, P., 1990. A new kinetic approach to modeling water-rock interaction: the role of nucleation, precursors, and Ostwald ripening. Geochim. Cosmochim. Acta 54, 2657–2677.

Strekopytov, S., Jarry, E., Exley, C., 2006. Further insight into the mechanism of formation of hydroxyaluminosilicates. Polyhedron 25, 3399–3404.

Wasylenki, L.E., Rolfe, B.A., Weeks, C.L., Spiro, T.G., Anbar, A.D., 2008. Experimental investigation of the effects of temperature and ionic strength on Mo isotope fractionation during adsorption to manganese oxides. Geochim. Cosmochim. Acta 72, 5997–6005.

Wasylenki, L.E., Weeks, C.L., Bargar, J.R., Spiro, T.G., Hein, J.R., Anbar, A.D., 2011. The molecular mechanism of Mo isotope fractionation during adsorption to birnessite. Geochim. Cosmochim. Acta 75, 5019–5031.

West, A.J., Galy, A., Bickle, M., 2005. Tectonic and climatic controls on silicate weathering. Earth Planet. Sci. Lett. 235, 211–228.

Wonisch, H., Gerard, F., Dietzel, M., Jaffrain, J., Nestroy, O., Boudot, J.P., 2008. Occurrence of polymerized silicic acid and aluminum species in two forest soil solutions with different acidity. Geoderma 144, 435–445.

Yokoyama, T., Nakamura, O., Tarutani, T., 1982. Polymerization of silicic acid adsorbed on aluminium hydroxide. Bull. Chem. Soc. Jpn. 55, 975–978.

Ziegler, K., Hsieh, J.C., Chadwick, O.A., Kelly, E.F., Hendricks, D.M., Savin, S.M., 2003. Halloysite as a kinetically controlled end product of arid-zone basalt weathering. Chem. Geol. 202, 461–478.

Ziegler, K., Chadwick, O.A., Brzezinski, M.A., Kelly, E., 2005a. Natural variations of delta Si-30 ratios during progressive basalt weathering, Hawaiian Islands. Geochim. Cosmochim. Acta 69, 4597–4610.

Ziegler, K., Chadwick, O.A., White, A.F., Brzezinski, M.A., 2005b. (DSi)-Si-30 systematics in a granitic saprolite, Puerto Rico. Geology 33, 817–820.